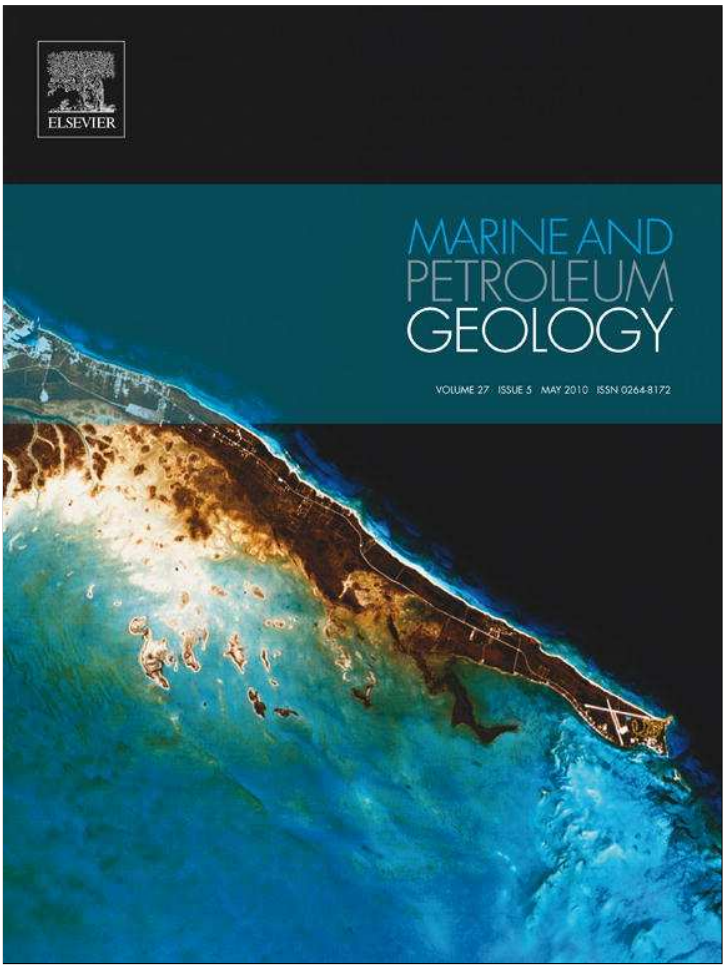

Marine and Petroleum Geology 27 (2010) 1133–1147

Contents lists available at ScienceDirect

Marine and Petroleum Geology

journal homepage: www.elsevier.com/locate/marpetgeo

Thermal regime of the northwest Indian rifted margin – Comparison with predictions

Gérôme Calvès [a,*], Anne M. Schwab [b], Mads Huuse [a,1], Peter D. Clift [a], Asif Inam [c]

[a] School of Geosciences, University of Aberdeen, Meston Building, Kings College, Aberdeen AB24 3UE, United Kingdom
[b] Marathon Oil U.K., Ltd, Marathon House, Rubislaw Hill, Anderson Drive, Aberdeen AB15 6FZ, United Kingdom
[c] National Institute for Oceanography, ST-47-Block 1, Clifton, Karachi 75600, Pakistan

ARTICLE INFO

Article history:
Received 3 October 2008
Received in revised form
5 January 2010
Accepted 14 February 2010
Available online 19 February 2010

Keywords:
West Indian Margin
Thermal regime
BSR
Volcanic margin
Rifting

ABSTRACT

We use a simple approach to estimate the present-day thermal regime along the northwestern part of the Western Indian Passive Margin, offshore Pakistan. A compilation of bottom borehole temperatures and geothermal gradients derived from new observations of bottom-simulating reflections (BSRs) allows us to constrain the relationship between the thermal regime and the known tectonic and sedimentary framework along this margin. Effects of basin and crustal structure on the estimation of thermal gradients and heat flow are discussed. A hydrate system is located within the sedimentary deep marine setting and compared to other provinces on other continental margins. We calculate the potential radiogenic contribution to the surface heat flow along a profile across the margin. Measurements across the continental shelf show intermediate thermal gradients of 38–44 °C/km. The onshore Indus Basin shows a lower range of values spanning 18–31 °C/km. The Indus Fan slope and continental rise show an increasing gradient from 37 to 55 °C/km, with higher values associated with the thick depocenter. The gradient drops to 33 °C/km along the Somnath Ridge, which is a syn-rift volcanic construct located in a landward position relative to the latest spreading center around the Cretaceous–Paleogene transition.

1. Introduction

The geothermal regime along the slope and deeper parts of the rifted western Indian passive margin is poorly constrained by direct measurements, such as temperature probes or deep penetrating boreholes. The deep crustal structure along this complex rifted margin is still under debate (Miles et al., 1998; Edwards et al., 2000; Minshull et al., 2008; Calvès et al., 2008a; Corfield et al., 2008; Henry et al., 2008). Nonetheless, recent drilling and seismic refraction studies now allow the location of the continent–ocean transition to be better constrained. As a result we can now directly compare crustal structure, sediment thicknesses and deposition rates with the modern geothermal system. Here we present for the first time a regional scale integrated study of the thermal regime using a compilation of different geophysical data.

An integrated interpretation of a terrestrial and marine data set, including deep crustal structure and heat flow, emerges as a potential way to relate observations at the solid Earth surface with deep-seated tectonic processes, such as lithospheric thinning, dynamic topography, or flow in the mantle. Since the publication of a simple model for the thermal regime of rifted margins by McKenzie (1978), numerous studies and models have addressed the processes of extension during the initiation and evolution of continental margins. Debate persists concerning the different origins of volcanic and non-volcanic margins, as well as the geometry of conjugate margins. Margin tectono-stratigraphy and thermal evolution during the pre-, syn- and post-rift periods have been the focus of particular study (White et al., 2003). The use of heat flow data to solve tectonic problems remains controversial. Most workers relate heat flow to tectonism and the thickness of the radiogenic crust. However, recently Goutorbe et al. (2008) have highlighted the role that mantle processes play in heat flow along continental margins. Here we address this by directly comparing heat flow and crustal structure across the rifted margin of Pakistan.

A review of measured heat flow from various sources in the Indian Ocean (Fig. 1A) highlights the lack of information in the study area. Most of the heat flow measurements in the deep NW Indian Ocean are located near the mid oceanic ridges and the Chagos-Laccadive Ridge (Fig. 1A and B). The Indo-Pakistani continental shelf has been sampled by limited oil exploration boreholes

* Corresponding author. Present address: Ifremer, Département Géologie Marine, Laboratoire Environnement Sédimentaires, 29280 Plouzané, France.
E-mail address: gerome.calves@laposte.net (G. Calvès).
[1] Present address: Basin Studies Group, SEAES, The University of Manchester, UK.

0264-8172/$ – see front matter © 2010 Elsevier Ltd. All rights reserved.
doi:10.1016/j.marpetgeo.2010.02.010

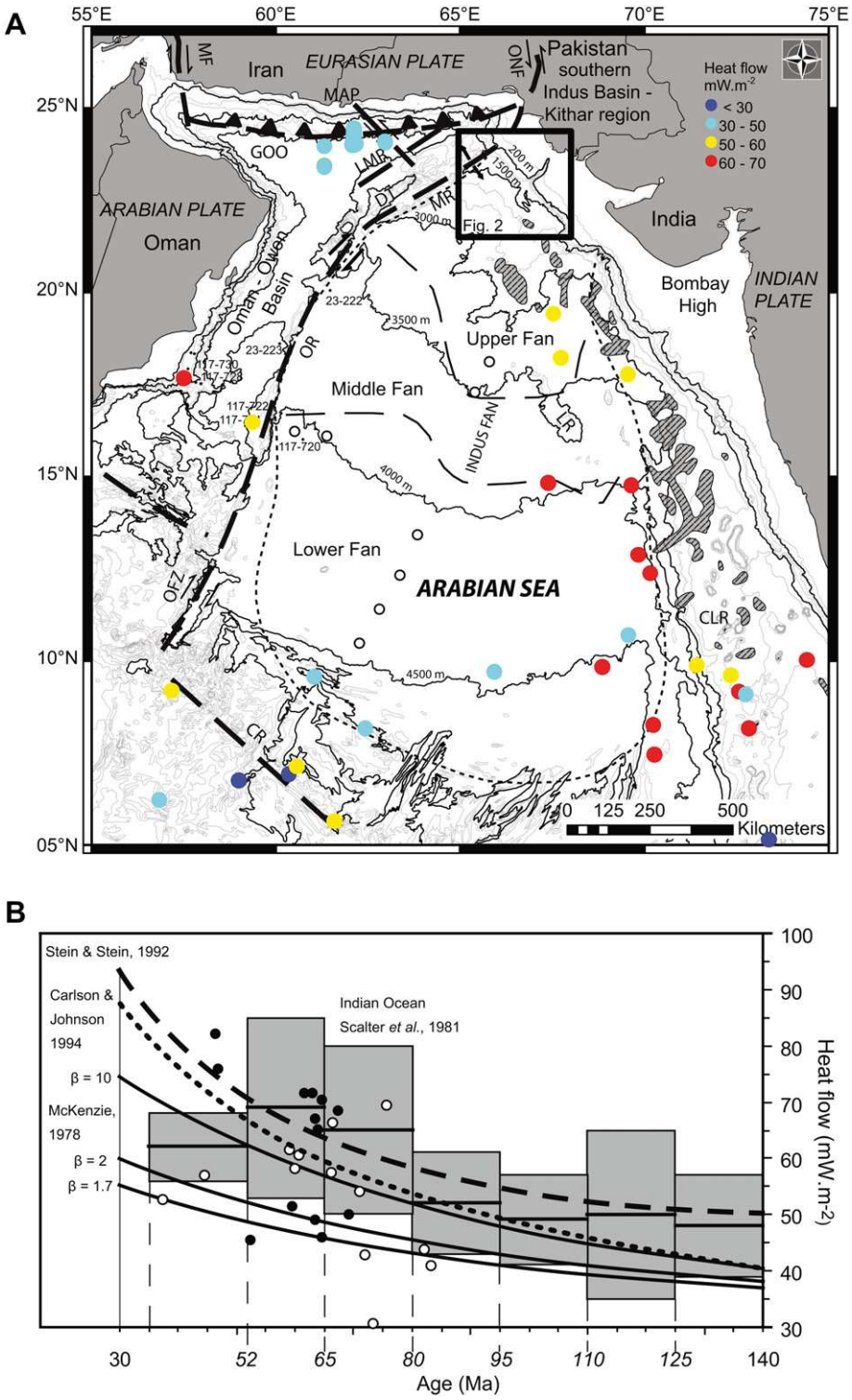

Fig. 1. A. Location map with main morphologic features of the Arabian Sea. The black box is the study area covered by reflection seismic data. The dashed dark line is the fringe of the Indus Fan (adapted from Kolla and Coumes, 1987; Droz and Bellaiche, 1991). The bathymetry data are from the GEBCO compilation. Scientific boreholes are from ODP Site Leg 117 (dark dots), DSDP Site Leg 23 (grey dots). Bold white dots on the axis of the Indus Fan are the location of sonobuoy data used by Bachman and Hamilton (1980). Zones of BSR previously identified on reflection seismic data are striped bodies along the Indian Margin (after Rao et al., 2002). Major structural features are abbreviated as: MR: Murray Ridge; OR: Owen Ridge; OFZ: Owen Fracture Zone; GOO: Gulf of Oman; MAP: Makran Accretionary Prism; SR: Sheiba Ridge; CR: Carlsberg Ridge; CLR: Chagos-Laccadives Ridge; LR: Laxmi Ridge. Heat flow values are from Pollack et al. (1993). B. Heat flow–age plot from measurements in the Indian Ocean (Sclater et al., 1981), for oceanic basins as predicted from GDH1 model (Stein and Stein, 1992) and from the uniform extension model (McKenzie, 1978) with a stretching factor of 1.7, 2 and 10. Heat flow values from the Chagos-Laccadive Ridge (black dots) and the Ninety-East Ridge (white dot) (Verzhbitsky, 2003).

mostly located south of the Indus Delta and in the Bombay High province. The deep-water Indus submarine fan itself suffers from a lack of heat flow measurements, except along its western edge where it has been sampled by Deep-Sea Drilling Project (DSDP) and Ocean Drilling Program (ODP) sites. However the onshore heat flow record is well constrained by Bottom-Hole Temperature (BHT) measurements from multiple water or mining wells within the Indian Shield and southern Indus onshore basin (Khan and Raza, 1986; Roy and Rao, 2000). This data set yields a wide variety of geothermal information across the NW Indian rifted margin. Following the study of basin thermal regimes, Robert (1988) classified basins into three types (basins with normal or near-normal paleogeothermal history, cooler than normal basins, and hotter than normal basins), with a geothermal gradient of 25–30 °C/km being indicative of basins with normal or near-normal paleogeothermal history in mature passive margin settings.

This study estimates the thermal regime of the NW portion of the Indian rifted volcanic margin and proposes links between margin tectonics, sedimentation and thermal evolution across this rifted volcanic margin.

1.1. Geological setting

The Indus Fan is the most extensive physiographic province in the Arabian Sea (Fig. 1A). This deep-sea fan sedimentary system is located at the triple junction of the Indian, Arabian and Eurasian Plates and is the second largest sediment body in the modern oceans. The fan is bounded by the rifted Indian continental margin, the Chagos-Laccadive Ridge on the east, the Owen-Murray Ridge to the northwest and west, and the Mid-Indian Ridge (Carlsberg Ridge) on the south. The Oman and the Owen Basins are the main physiographic features in the westernmost Arabian Sea (Kolla and Coumes, 1987).

The plate tectonic organization of the NW Indian Ocean reflects the multiphase break-up history between Africa, Madagascar, the Seychelles and India associated with extensive magmatic activity and the subsequent collision of India with Eurasia at around 50 Ma (Norton and Sclater, 1979; Gombos et al., 1995). The break-up of eastern Gondwanaland started at 150 Ma between the Africa–Somalia plates and the Madagascar–Australia blocks, followed by the separation of the Indian Plate and the Antarctica–Australia block at the Jurassic–Cretaceous boundary ($\sim 128 \pm 2$ Ma) (Gaina et al., 2007). Around 85–90 Ma Seychelles–India separated from Madagascar and created the Mascarene Basin (Storey et al., 1995). The Seychelles–India block migrated north with the opening of the Laxmi Basin starting at 67 Ma (Royer et al., 2002), which was followed by the eruption of the Deccan continental flood basalts ~65 Ma (e.g. Bernard and Munschy, 2000; Courtillot et al., 2000; Collier et al., 2008 and references within).

The large volume ($\sim 5.0 \times 10^6$ km^3) of sedimentary material sitting within and south of the present-day Indus Delta is shown by the sediment two-way time thickness (TWT) map (Fig. 2), with thicknesses estimated to reach ~11 km (Naini and Kolla, 1982; Kolla and Coumes, 1987). The study area is located between the continental shelf of Pakistan, the Murray Ridge and the Somnath Ridge, which is a volcanic feature in the crustal continent–ocean transition zone, whose continental versus oceanic character has been debated (Malod et al., 1997; Gaedicke et al., 2002; Clift et al., 2002; Minshull et al., 2008) (Fig. 2). The Indus Fan is the principle sedimentary depocentre of the Western Himalaya–Karakoram region since the Eocene, with peaks of sedimentation in the Middle Miocene (Clift and Gaedicke, 2002; Clift, 2006) and Plio-Pleistocene times (Métivier et al., 1999).

The study area is defined by three main types of tectonic boundaries. To the northeast the area is limited by a growth fault

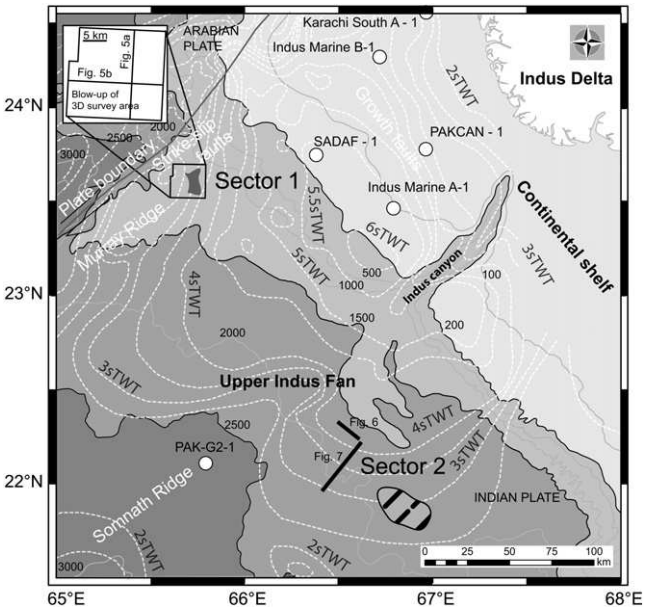

Fig. 2. Sedimentary-structural and bathymetric map GEBCO Digital Atlas (British Oceanographic Data Centre, 2003) of the study area west of the Indus Delta (Fig. 1A). Exploration boreholes are located by white dots. Tectonic domains are related to three major regional constraints: strike-slip motion along the plate boundary at the Murray Ridge in the NW, growth faults due to sediment loading along the continental shelf in the NE, and the Somnath Ridge related to a volcanic edifice under the Upper Indus Fan in the SW. A major depocenter is located at the shelf to slope transition and the Indus Canyon (Kolla and Coumes, 1987). The locations of seismic figures illustrating bottom-simulating reflections (BSRs) are shown: Fig. 5 in Sector 1 of the 3D seismic survey and 2D seismic line Figs. 6 and 7 in Sector 2.

regime on the continental shelf, while to the northwest is a strike-slip plate boundary along the western edge of the Murray Ridge, and to the southwest lies the volcanic Somnath Ridge, which is draped by the Upper Indus Fan (Fig. 2). Here we focus on two sectors where we have good data control. These two sectors represent areas where bottom-simulating reflectors (BSR) and potential gas hydrates are recognized by seismic reflection profiles and are used in this study to constrain the geothermal gradient. In Sector 1 (Fig. 2), the seafloor dips to the south with water depths ranging from 1040 to 1325 m, whereas in Sector 2 the seafloor slopes to the southwest from 1587 to 2086 m. The overall slope gradient is 0.6–0.7° at both locations (Fig. 2).

The northernmost portion of the western Indian rifted margin lies between continental crust (onshore-continental shelf), and an ocean–continent transition zone with volcanic rocks (Somnath Ridge). To the south the oldest known magnetic anomaly related to oceanic crust is An 28 (~63 Ma) and is located west of the Laxmi Ridge (Royer et al., 2002). The crustal thickness of the Indian Shield ranges from 32 to 45 km just south of the study area to a total lithospheric thickness of between 85 and 120 km estimated from deep seismic sounding and/or gravity modeling in the center of the shield (Todal and Eldholm, 1998; Walter et al., 2000; Surya Prakasa Rao and Tewari, 2005; Kumar et al., 2007). Along the distal portion of Murray Ridge (presumed to be a continental block, Edwards et al., 2008), the Moho discontinuity is estimated to be as deep as 18 km ± 1 from gravity modeling (Gaedicke et al., 2002), and wide-angle seismic data allows a depth to Moho to be modeled to about 18–23 km on the SW portion of the ridge (Edwards et al., 2008). A recent wide-angle seismic experiment between the Somnath Ridge and the Laxmi Ridge estimated the depth to Moho at 22 ± 2 km and 20 ± 5 km respectively (Lane, 2006; Minshull et al., 2008).

1.2. BSR and hydrates along the North and East margins of the Arabian Sea

Two major locations have been classified as gas hydrate occurrences along the margins of the Arabian Sea (Kvenvolden and Lorenson, 2001), as inferred from the presence of BSRs in the shallow subsurface (Fig. 1). These two provinces are located on the Indian Continental Slope (Veerayya et al., 1998; Rastogi et al., 1999; Rao et al., 2001) and in the Makran Accretionary Prism (MAP in Fig. 1) (White, 1977; Minshull and White, 1989; Grevemeyer et al., 2000; Kaul et al., 2000; Von Rad et al., 2000; Sain et al., 2000). Recently a BSR was also recognized in the Indus Fan region (Calvès et al., 2008b).

The range of water depths at which BSRs occur in the Makran Accretionary Prism is 500–3000 m (Kaul et al., 2000), while the estimated maximum depth of BSRs below the seafloor is 500–800 m (Von Rad et al., 2000; Grevemeyer et al., 2000). Along the Indian Margin, the occurrence of BSRs or gas-charged amplitude anomalies is confined to water depths ranging from 500 to 3000 m, and depths below the seafloor up to 450 m (Rao et al., 2002; Shankar et al., 2004, 2006). No gas hydrate samples have been recovered from cored sediment in the Arabian Sea. The source of methane and gases at these locations is thought to be related to deep thermogenic gas formation (Rastogi et al., 1999; Grevemeyer et al., 2000; Satyavani et al., 2005; Calvès et al., 2008b).

1.3. Heat flow along the NE Arabian Sea margins

Only a few of the data points in the world heat flow data set compiled by Pollack et al. (1993) were derived along the western Indian margin, where values are known to range from 67 to over 70 mW m^{-2}. The predicted heat flow, based on an integrated heat flow database and 3D global seismic shear velocity model for the western rifted margin of India, ranges from 50 to 80 mW m^{-2} (Shapiro and Ritzwoller, 2004).

Thermal gradients are estimated assuming a linear trend from bottom-hole temperature measurements in boreholes or from the depth of seismic reflections associated with BSRs in the shallow subsurface. Here we present heat flow values from the margin, starting with the continent and continuing into the deep basin. Onshore in the Kirthar region (southern Indus Basin – Fig. 1) the geothermal gradient ranges from 18 to 31 °C/km with an average of 24.5 °C/km (Khan and Raza, 1986), these values are measured from BHT (bottom-hole temperature) and are not corrected for formation temperature (Table 1), which can introduce an important source of uncertainty to the real heat flow value (Hutchinson, 1985). To the south, the Deccan Volcanic Province along the western margin of India shows low heat flow values ranging from 31 to 50 mW m^{-2} (Roy and Rao, 2000). Interestingly, these authors note that the present-day heat flow south of the Deccan Volcanic Province does not show evidence of the thermal effects associated with Cretaceous–Tertiary Deccan volcanism (discussed further below). On the continental shelf, measured geothermal gradients from boreholes indicate values of 37.9–43.6 °C/km – offshore Pakistan (Shuaib and Shuaib, 1999). The mean value of 41.4 °C/km (~50 mW m^{-2}, for a thermal conductivity of 1.2 W m^{-1} K^{-1}), which is indicative of an average thermal regime along the continental shelf when compared with compiled values (50 ± 15 mW m^{-2}) along equivalent passive margin settings (Allen and Allen, 2005). The thermal regime close to the ocean–continent transition in the deeper part of the margin is unknown, with the exception of a recent petroleum exploration borehole PAK-G2-1 located on the crest of the Somnath Ridge (Fig. 1), which penetrated an isolated carbonate platform. This hole recorded a relatively low geothermal gradient of 33.5 °C/km (bottom-hole temperature not corrected for thermal conductivity variation). Heat flow studies have been carried out along the Makran Accretionary Prism using computed estimates from BSRs and in situ measurements (Kaul et al., 2000; Delisle and Berner, 2002). The heat flow values measured in the Makran Accretionary Prism are between 24 and 60 mW m^{-2}, with a mean thermal conductivity value of 1.27 W m^{-1} K^{-1} (Kaul et al., 2000).

Table 1
Geothermal gradient measurements from boreholes in the Arabian Sea (Shuaib and Shuaib, 1999), onshore (Khan and Raza, 1986) and derived from the depths of BSRs this study.

Borehole	Total Depth (m)	Geotherm (°C/km)	Domain	Depth to basement (m)
Khan and Raza, 1986				
Kithar region	_	18–31	Indus Basin	~3000–5000
Shuaib and Shuaib, 1999				
Indus Marine A-1	2841	42	Continental shelf	>7000
Indus Marine B-1	3804	44		~5500
Pakcan-1	3701	38		~5500
Dabbo Creek-1	4354	39		~5000
This study				
Pak-G2-1	4750	33	Deep water	5875
Sector 1	BSR depth	39		~5036
Sector 2	BSR depth	50		8648

2. Data set and estimation of geotherm from BSR depth

The database used for this study is a compilation of information from seismic reflection surveys, seismic stacking velocities, physical properties (i.e. porosity, thermal conductivity, and downhole temperature measurement), oceanographic water column measurements (i.e. conductivity, temperature and depth – CTD profiles), geochemical measurements (i.e., gas type, concentration) from DSDP–ODP sites drilled into the Indus Fan and recent industrial exploration boreholes. Crustal thickness estimates from published works were employed as further constraints to the geodynamic setting with which the heat flow value can be compared.

The occurrence of BSRs related to methane hydrates in the shallow subsurface allows us to estimate the thermal regime because hydrates are only stable in a very limited range of temperatures and pressures (Yamano et al., 1982; Sloan, 1998).

2.1. Geophysical data set

The seismic data set covers most of the margin in the offshore Pakistan territorial area. Boreholes used in this study are located on the continental shelf, slope and toe of the Indus Fan (both industrial exploration and scientific). The seismic data used for the current study are 2D and 3D multi-channel, post-stack, time-migrated reflection seismic surveys data (Fig. 2).

The 2D seismic data lines of Sector 2 shown in this paper are 160-fold, with a 4 ms two-way travel time (TWT) sample rate. These data were acquired in 2000, with a frequency range of 5–90 Hz and a grid spacing ranging from 5 to >25 km. The 3D seismic survey of Sector 1 covers an area of 375 km^2 and is 120-fold with a 4 ms TWT sample rate. The 3D grid is subdivided into inline and crossline directions, spaced at 25 m and 12.5 m respectively. The frequency range in the shallow subsurface is 7.5–90 Hz, with a dominant frequency in the 25–50 Hz range. Assuming a dominant frequency around 30–40 Hz and a velocity of 1800 m/s, the

vertical seismic resolution, defined as a quarter of the dominant wavelength, would be around 10 m.

2.2. Physical properties of the Arabian Sea

In the study area, the seafloor depth ranges from 1040 to 1325 m in Sector 1 (the area covered by the studied 3D seismic data, as shown in Fig. 2) and 1587–2086 m in Sector 2. Assuming hydrostatic pressure, the pressure at the seafloor in Sector 1 is 105–133.5 Bar and in Sector 2 is 159–209 Bar respectively (Fig. 2) for each sector. The bottom-water temperature used in this study is a function of depth, and is not a constant value for a wide range of depths. Therefore, seasonal effects and/or bottom currents are smoothed out by using a compilation of CTD profiles from the study area within the Arabian Sea (grey dots in Fig. 3) (World Ocean Database 2005 – http://www.nodc.noaa.gov/OC5/WOD05/pr_wod05.html). This 30 year record from CTD surveying shows that bottom-water temperatures lie between 3 and 8 °C, with a variation of less than 0.5 °C at a constant depth (Fig. 3). Variations in bottom-water temperature can affect the geothermal gradient and the heat flow calculated from the thickness of the hydrate stability zone. The two primary conditions of high pressure (i.e. high water depth) and low temperature are present in the study area, which is thus appropriate necessary for the formation of gas hydrates, assuming a source of fluids (i.e. water, methane, CO_2) in the shallow subsurface (Sloan, 1998), are present in the study area (Fig. 3).

Rock thermal conductivity values are not available for the study area. As a result we have used a regional compilation of published data, as well as unpublished data of restricted access from the Arabian Sea (Fig. 3) (162 measurements – probe and downhole measurements) (Pollack et al., 1993; http://www.heatflow.und.edu/index2.html). Two peak values can be inferred from this compilation, a first at 0.8 $W\,m^{-1}\,K^{-1}$ and a second at 1.17 $W\,m^{-1}\,K^{-1}$. Because this range of values is comparable to other passive margins (Grevemeyer and Villinger, 2001) we have chosen to follow a conservative 1 $W\,m^{-1}\,K^{-1}$ solution for the shallow subsurface of the study area. This makes the use of geothermal gradient and heat flow equivalent. The raw data appear in the units at time of measurements (Table 1).

2.3. Velocity–depth and porosity–depth curves

To convert the seismically derived TWT values derived from the seismic data into depth we use a time–depth function extracted from a stacking velocity and an interval velocity model (Fig. 4):

$$z = 179.05t^2 + 762.22t - 1.0816,$$

where z is the depth of the seismic reflection associated with the BSR measured below the seafloor and t is the two-way time–depth of the BSR below seafloor (TWT). The water depth is computed from seafloor reflection TWT values and a seawater velocity of 1500 m/s. An uncertainty of 20% on the depth of the BSR below seafloor is expected from our depth conversion, assuming that this is comparable to the predicted base of the hydrate stability zone (BHSZ) calculated from the measurement of heat flow (Ruppel, 1997; Lucazeau et al., 2004).

The study area time–depth curve is compared to a reference curve, the Bachman and Hamilton curve (1980) derived from sonobuoy data on the Lower Indus Fan (Figs. 1 and 4), and shows 1–16% lower velocity. The velocity–depth function used for the study area implies a decrease of velocity of 1–16% from the regression curve published by Bachman and Hamilton (1980) on the Lower Indus Fan.

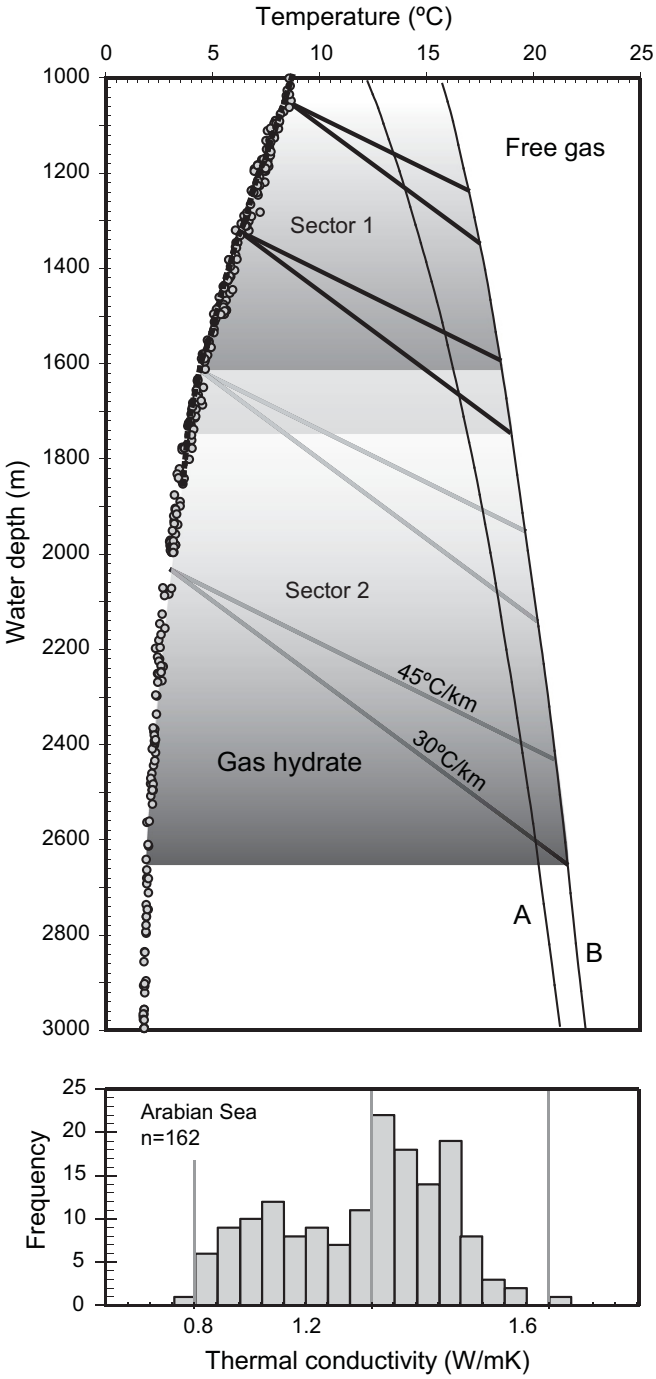

Fig. 3. Stability conditions for gas hydrate from depth–temperature readings within Sectors 1 and 2 of the study area. Seawater temperature data compiled from CTD–NODC database measured in the Arabian Sea (grey dots). A CTD profile from NOC Southampton is used as reference for the study area (dark line). The theoretical curves are calculated using seawater–methane approximation with 100% methane (curve A) and 96% methane, 3% ethane and 1% propane (curve B) with the program of Sloan (1998). Thermal conductivity frequency plot of sediments measured (n = 162) in the Arabian Sea.

The porosity–depth curve from is plotted with reference to DSDP Site 222 (Fig. 4; (Whitmarsh et al., 1974)) in order is used to show the variations of porosity within the shallow subsurface. Because the study area is in a more proximal position on the Indus Fan than DSDP Site 222 (Fig. 1A), we suggest that the sediments might be composed of less clay and/or pelagic carbonate, and

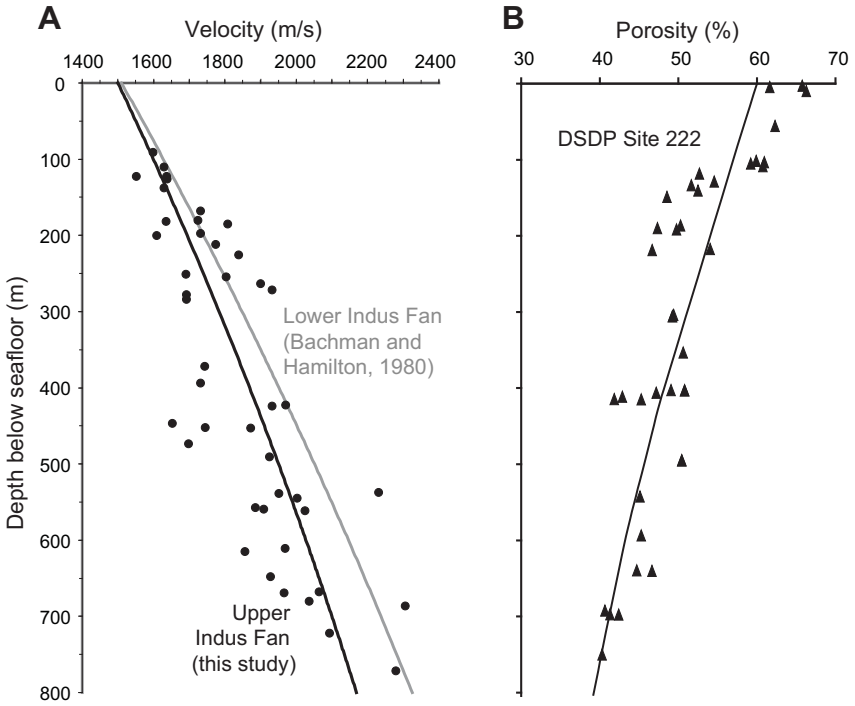

Fig. 4. A) Depth velocity profile. The black dots are calculated from seismic interval velocities. The bold black curve is the best fit curve estimated from the stacking velocities. These velocities are compared to the Lower Indus Fan regression function for clastic sediments – grey curve (Bachman and Hamilton, 1980). B) The porosity–depth curve profile is from DSDP site 222 shows the variation of porosity within the shallow subsurface (Bachman and Hamilton, 1976).

therefore that the velocity profile might be less steep compared to the distal section (porosity or lithology). Another important factor affecting the velocity will be the porosity variation between proximal versus distal sites on the fan (Wyllie et al., 1956; Erickson and Jarrard, 1998). It has been shown on recent and modern deep-sea fans (e.g., Amazon Fan) that the influence of facies on velocity and density, and thus on seismic reflection images, is only indirect, i.e. via their effect on porosity (Erickson and Jarrard, 1998). The initial porosity and progressive loss during compaction and burial provides a way to understand velocity variations in sedimentary basins, but such variations are difficult to incorporate into basin modeling (Giles et al., 1998). Additional factors affecting the time–depth conversion include the effects of rapid sedimentation rates in regions that part of the margin and/or the resultant potential overpressure (Gardner et al., 1974; Japsen et al., 2007).

2.4. Geothermal gradient estimation from BSR depth

Variations in the thermal regime of sedimentary basins can be a good indicator of tectonic features and/or fluid migration through the sedimentary pile. The depth of the BSR or BHSZ can be used to compute heat flow using the known stability range of hydrates and the thermal conductivity of the host sediments (Yamano et al., 1982; Cande et al., 1987; Hyndman and Spence, 1992; Grevemeyer and Villinger, 2001; Vanneste et al., 2002). This estimation is based on the assumption that the BSR is related to the BHSZ. The workflow consists of the following steps: (1) Conversion from TWT to depth based on the velocity model derived from stacking velocities of the reflection seismic data within the study area, (2) computation of the pressure at the depth of the observed BHSZ, and (3) determination of the geothermal gradient or heat flow based on the temperature at the BHSZ and the temperature of the water at the seafloor.

3. Interpretation

3.1. P–T conditions at the study area – hydrate stability field

The hydrate stability curves for the study area (Fig. 3) are calculated using the CSMHYD program of Sloan (1998) assuming hydrostatic pressure. In order to assess potential uncertainties due to gas composition we use both the seawater approximation with 100% methane (curve A in Fig. 3) and with 96% methane, 3% ethane and 1% propane (curve B in Fig. 3). We then use a common average geothermal gradient of 30–45 °C/km for a continental margin to estimate the approximate expected depth of the hydrate stability zone, and therefore the potential depth of the BSR below the seafloor. The temperature at the seafloor is estimated from CTD profiles in the Arabian Sea (Fig. 3). In the two sectors, hydrate is predicted to be stable in sediment from 116 to 625 m below seafloor, based on a hydrate stability field for scenarii A and B and assuming a 30–45 °C/km geothermal gradient and water depths of 1050, 1325, 1620 and 2035 m. Our results are summarized in Table 2.

3.2. Seismic evidence for BSR and potential free gas

BSR and potential bright spots related to free gas are observed in the two sectors of the study area in water depths of 1050–2035 m.

Table 2
Scenario of base of hydrate stability zone below seafloor for given water depths, different gas composition, and geothermal gradient.

Water depth (m)		1050		1325		1620		2035	
Temperature at seafloor (°C)		8.4		6.3		4.5		3	
Gas composition		A	B	A	B	A	B	A	B
BHSZ mbsf	30 °C/km	186	345	345	421	465	530	570	625
geotherm	45 °C/km	116	215	215	270	295	335	370	400

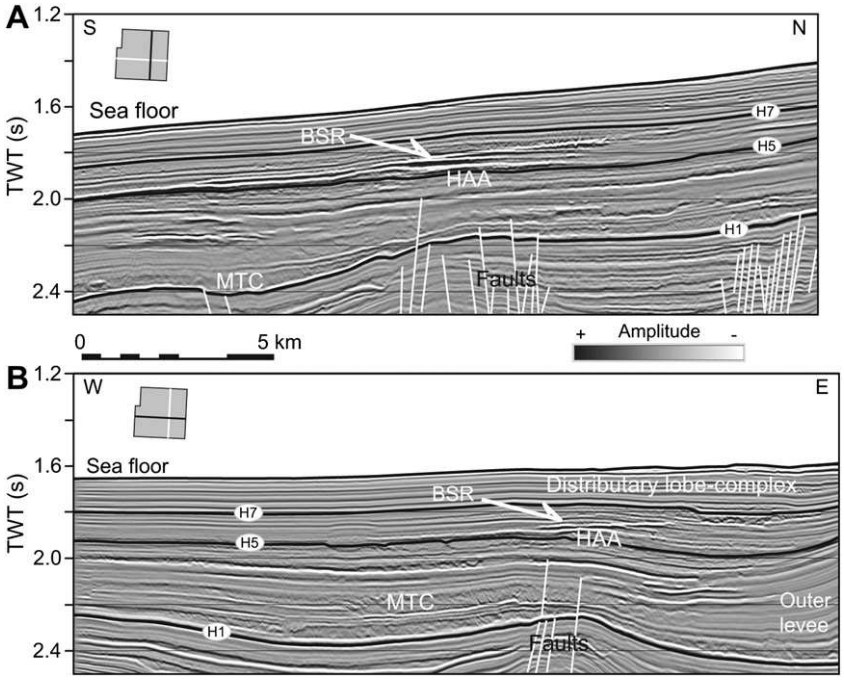

Fig. 5. Seismic sections from 3D reflection seismic survey showing evidence of BSR cross-cutting reflections – Sector 1 (S–N: (A), W–E: (B)). The main amplitude anomaly (HAA) is related to the BSR-potential free gas sitting above a strongly faulted high in a lobe depositional system. Seismic facies are related to slope sedimentary processes such as a distributary lobe-complex, outer-levee and mass transport complex (MTC). Stratigraphic horizons are equivalent to those described in Calvès et al. (2008b). HAA: high-amplitude anomaly.

Sector 1 is part of a 3D seismic reflection survey on the slope of the margin along the eastern edge of the Murray Ridge (Calvès et al., 2008b) (Fig. 2). Sector 2 is part of a 2D seismic reflection survey in the Upper Indus Fan between the most recently active Indus Canyon and the Somnath Ridge.

High-amplitude reflections are identified on two sections between two continuous stratigraphic horizons H5 and H7. These discontinuous reflections (0.2–15 km long) occur 200–300 ms TWT below the seafloor (high amplitude: HA – Fig. 5). They have reversed polarity compared to the seafloor reflection, indicative of a strongly negative acoustic impedance contrast, typical of a gas hydrate accumulation (Shipley et al., 1979). These high-amplitude reflections cross-cut the background parallel reflections, which are associated with a lobe depositional system. These characteristics strongly suggest that the bright reflections are associated with a BSR. However, this BSR is weak compared to classic BSRs observed along many other margins (Shipley et al., 1979; Vanneste et al., 2001). The sedimentary environment hosting the BSR and associated hydrates is related to distributary lobe-complexes, which are prone to being good fluid reservoirs, compared to the background parallel-bedded, muddy, turbidite sediments (Calvès et al., 2008b).

A 'classic' BSR with reverse polarity compared to the seafloor reflection and cross-cutting the stratigraphy is observed in Figs. 6 and 7, respectively strike and dip sections. The BSR is expressed by discontinuous reflections (0.55–5.5 km long) occurring 300–450 ms TWT below the seafloor. In Fig. 6 the main BSR is seen to be located at the top of a channel–levee and cross-cuts the upper channel infill of the axis of the channel, The BSR is depicted by bright amplitudes, i.e., potential free gas in porous facies. Two other smaller, individual BSRs are identified towards the southwest southeastern end of the profile (Fig. 6), at the shoulders of a sequence of reflections draping an incision inside an inner levee. Along the NE–SW profile (Fig. 7) as the seafloor is undulating and deepening, the BSRs are observed to clearly cross-cut the host sedimentary system, which is a channel–levee complex. A high-amplitude BSR is located at the top of an inner levee and on the edge of the shoulder of a scalloped outer-levee in the northeast end of the profile. High-amplitude reflections (HARs) in Figs. 6 and 7 are related to the channel in the channel–levee complex. This seismic facies might represent a sandy, reservoir prone lithology and thus a suitable host for hydrocarbons. This might explain the location of a strong BSR on top of the channel facies as compared to the muddier levee facies.

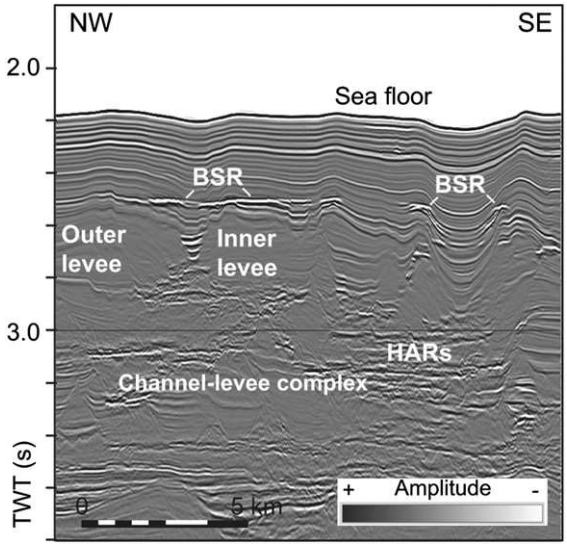

Fig. 6. NW–SE seismic section from 2D reflection seismic showing evidence of BSR cross-cutting reflections – Sector 2. Disrupted BSRs are depicted on this line in a cross-cutting geometry at the top of a channel–levee complex. Seismic facies are related to channel–levee systems at the base of the slope, high-amplitude reflections (HARs) in a channel, and outer and inner levees. Section location is shown in Fig. 2.

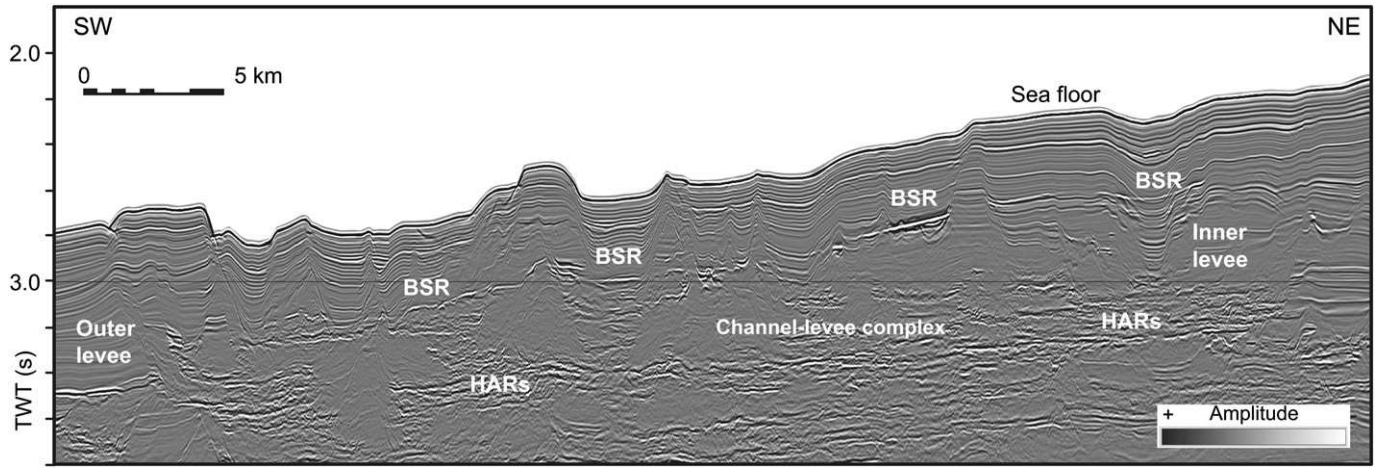

Fig. 7. SW–NE seismic section from 2D reflection seismic showing evidence of BSR cross-cutting reflection – Sector 2. Disconnected BSRs are depicted on this line in a cross-cutting geometry at the top of channel–levee complex and inside the core of channel. Seismic facies are related to channel–levee systems at the base of the slope, high-amplitude reflections (HARs) in a channel, and outer and inner levees. Section location is shown in Fig. 2.

3.3. Estimated geothermal gradient from depth of BSR

From Sectors 1 and 2 we use the BSR depth to constrain the thermal regime at these locations (slope or base of slope). In Sector 1 the water depth ranges from 1049 to 1325 m (Fig. 8A). The BSR observed in the shallow subsurface (Fig. 5A and B) is mapped in detail from the 3D seismic data set (ranging from 140 to 225 m below seafloor) (Fig. 8B). A confidence area, outlined by with a white dotted line, contains the occurrences of BSR and bright, high-amplitude reflections (Fig. 8B and C). The geothermal gradient is estimated from the methodology explained above and then mapped and extrapolated across the mapped BSR (Fig. 8C). Geothermal gradient values are 37.2–46.7 °C/km. Fig. 8D compiles the different sets of geological and geothermal information. Three tectonic blocks (α, β, χ) are depicted from a seismic coherency image at Horizon H1 (Fig. 5) that shows the fault geometry and reveals a zone of focused gas flow related to a structural high (anticline), which is located below the bright event, high-amplitude events caused by the presence of a BSR and potential free gas in the center of the 3D survey (Fig. 8D). In the zone outlined by the white dotted line the geotherm estimated from the BSR slightly increases. This could indicate potential heat transport that would cause the BSR to shallow at the apex of this anticline.

In Sector 2, only two 2D seismic lines display discontinuous BSRs (Figs. 6 and 7). Estimates of the geothermal gradient have been carried out along these lines, where the BSR is present. The geothermal gradient estimate ranges from 44 to 55 °C/km. Overall, it is seen that as water depth increases so does the geothermal gradient (Fig. 9).

3.4. Influence of sedimentation on BSR depth and thermal gradient estimation

There has been very low to no active clastic sedimentation within the study area since the Younger Dryas (~11 ka), with potential erosion limited to the edge of the shelf, Indus Canyon and the edge of the Murray Ridge (Von Rad and Tahir, 1997). We use the same approach as Martin et al. (2004) to estimate the effect of given sedimentation rates on the fluctuation of the thermal gradient, assuming a purely sedimentary scenario (i.e. no erosion) and accounting for the potential thermal blanketing effect of rapid sedimentation.

Sedimentation rates are based on known drilled age constraints and projected stratigraphic models at other locations in Sectors 1 and 2 (Fig. 10). The results are shown presented in a proximal to distal direction:

- PW-Sector 1 and PW-Sector 2 sedimentation rates are inferred from the seismic stratigraphic framework (Reflector H7 ~ 1.8 Ma, Reflector H5 ~ 2.6 Ma and Reflector H1 ~ 6.5 Ma) and vary sequentially from 72 ± 4, to 159 ± 28 to 82 ± 25 m/m.y.,
- PAK-G2-1, in the Upper Indus Fan, has sedimentation rates of 95 m/m.y. between the seafloor and the 1.6 Ma, horizon and 185 m/m.y. from 1.6 to 3 Ma,
- DSDP Site 222, in the middle part of the Indus Fan, has sedimentation rates of 48 m/m.y. between the seafloor and the 1.6 Ma horizon, 228 m/m.y. from 1.6 to 3 Ma, 120 m/m.y. from 3 to 5 Ma, and 453 m/m.y. from 5 to 6.5 Ma (Whitmarsh et al., 1974),
- ODP Site 720, in the distal portion of the Indus Fan (middle to lower fan), has sedimentation rates of 31.6 m/m.y. between the seafloor to 0.2 Ma, 136 m/m.y. from 0.2 to ~0.73 Ma, 944 m/m.y. from 0.73 to ~0.84 Ma, and 196 m/m.y. from 0.84 to ~1.23 Ma (Prell et al., 1989).

From these estimates of sedimentation rates along the margin and the Indus Fan, we calculate an average sedimentation rate of 100 m/m.y. in the last 3 m.y. at the location of the observed BSRs (PW-Sectors 1 and 2 in Fig. 10). Because the present-day observed BSR is assumed to be at equilibrium, the 100 m of sediment deposited since 1 Ma will have affected the BSR depth and geotherm by less than 25 m in water depths of 1900 m (Sector 2). In turn this implies a thermal blanketing of only 0.45 °C/100 m for an average geothermal gradient of 37.5 °C/km. In shallower water, as in Sector 1, the effect of the same sedimentation trend would imply more significant blanketing on the geotherm of 0.8 °C/100 m and a BSR depth variation of about 40 m because the hydrate stability field (Sloan, 1998) is more sensitive to pressure variations in this range water depth (1000–1300 m).

3.5. Predicted heat flow from model

In this section we use McKenzie's (1978) uniform extension model to predict heat flow after rifting and compare this with our

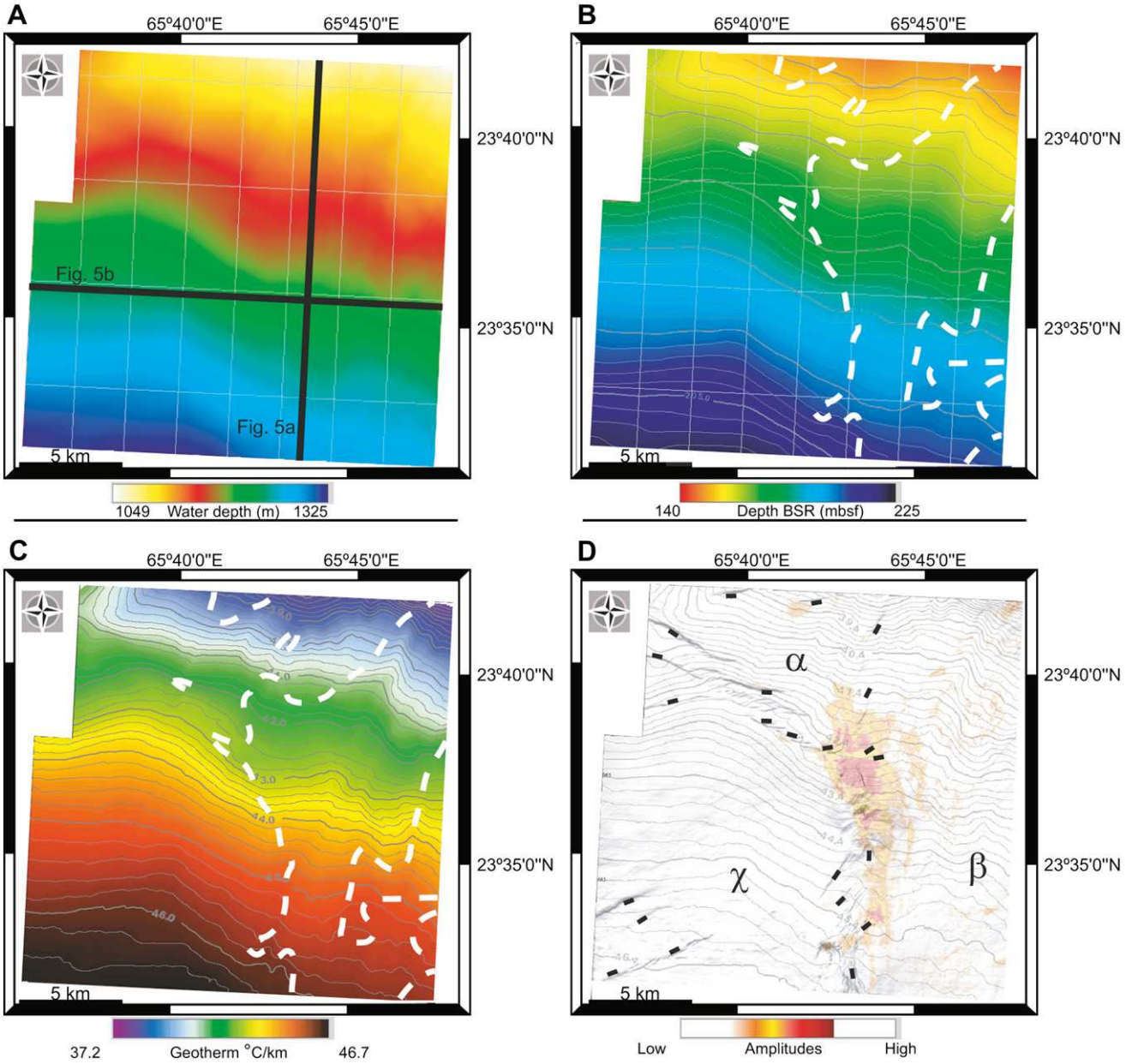

Fig. 8. Results from a detailed analysis of the base of hydrate stability zone (BHSZ) within the 3D seismic data set – Sector 1. (A) Water depth map (m) assuming 1500 m/s seawater velocity. (B) Depth of the BSR below seafloor (m), where dotted white lines outline the confident areas where the top of the BSR-free gas interval is equivalent to the BHSZ. (C) Inferred geothermal gradient (°C/km) from the HSZ thickness. (D) Coherency extraction of the Horizon H1 to illustrate the strong relationship between the focused fluid flow and the increase of heat in the vicinity of faults and folds (black lines). The high amplitude related to the free gas and BSR in the interval H7–H5 is draped on top. The three tectonic blocks related to the strike-slip setting are α, β, and X. Fig. 5 shows Horizons H1, H5 and H7 on a seismic line.

measurements. Although extension may not have been perfectly uniform there is no suggestion of Iberia-style detachment faults offshore Pakistan and so this simple model is a reasonable first-order estimate with which to compare measurements. A lithospheric stretching factor (β) profile for each location has been determined from the present-day crustal thickness (y_1) by assuming that the pre-rift crustal thickness (y_0) is known and uniform. The crustal stretching factor (β) is given by the following equation:

$$\beta = y_0/y_1.$$

The thermal regime is not corrected for the contribution from radiogenic heating. Pre-rift crustal thickness (y_0) for each point has been determined from the maximum value along its length and is typically 32 km (MENA 1.1, Walter et al., 2000). This thickness is preferred for this case study over the global average of ~35 km from Christensen and Mooney (1995). Using a 35-km-thick original crust implies a variation of about 10% on the stretching factor estimation. Observed modern crustal thicknesses in the study area – continental shelf to slope of the margin – range from 27 to 22 km. The depth to basement is measured from the seismic basement, which is of 65 Ma age. Results from of the computed heat flows (Table 3) are plotted in Fig. 11 with a cross plot of stretching factor versus measured or computed geothermal gradient at the different locations. The range of stretching factors (β) along the margin based on the present-day crustal thickness is 1.6–2.4 (Fig. 11). Because the stretching factor is higher than 1.5, the

Table 3
Average values used to compute stretching factor and predicted heat flow for study area using the McKenzie model.

Location	Depth to basement (average) (km)	y_0 (km)	y_1 (km)			Predicted heat flow for rifting at 65 Ma (mW m^{-2})	Measured geotherm (°C/km)
			22 β_1	25 β_2	27 β_3		
Continental shelf	5.62	32	2.01	1.69	1.53	44.9 ± 1.5	41
Sector 1	5.04		1.89	1.60	1.46	44.7 ± 1.5	39
Sector 2	8.65		2.4	1.96	1.74	48.4 ± 2	50
Deep water	5.87		1.98	1.67	1.51	52.1 ± 8.5	33

heat flow anomaly computed with the McKenzie model will be reliable even if it has been more than 30 m.y. since rift break-up. If there has been igneous addition (<5 km) to the continental crust during extension then β would be reduced compared to the estimate of McKenzie (1978). The result is a prediction of heat flow caused by a rifting event at 65 Ma of 44.9–59.1 mW m^{-2}, along a proximal to distal profile of the margin.

4. Discussion

4.1. Variation of hydrate system along a continental margin

The two sectors of the Indus Fan that we examined in this study show a variety of sedimentary host systems and contrasting tectonic settings. However, these two systems sectors are only separated by ~160 km (Fig. 2). Sector 1 is affected by gravity spreading and a strike-slip tectonic regime, while Sector 2 is a quiet, passive tectonic regime with a higher rate of sedimentation. These two deep-water sedimentary systems contain potential reservoirs for the fluids that source the hydrate phase in the sediments. The Indus Fan comprises contains a high percentage of silty–clayey sediments, with potential sandier facies associated with channel–levee systems or lobes (Deptuck et al., 2003; Calvès et al., 2008b) (Figs. 5a,b, 6 and 7). The location of the observed BSRs appears to be related to the presence of coarser sedimentary reservoirs.

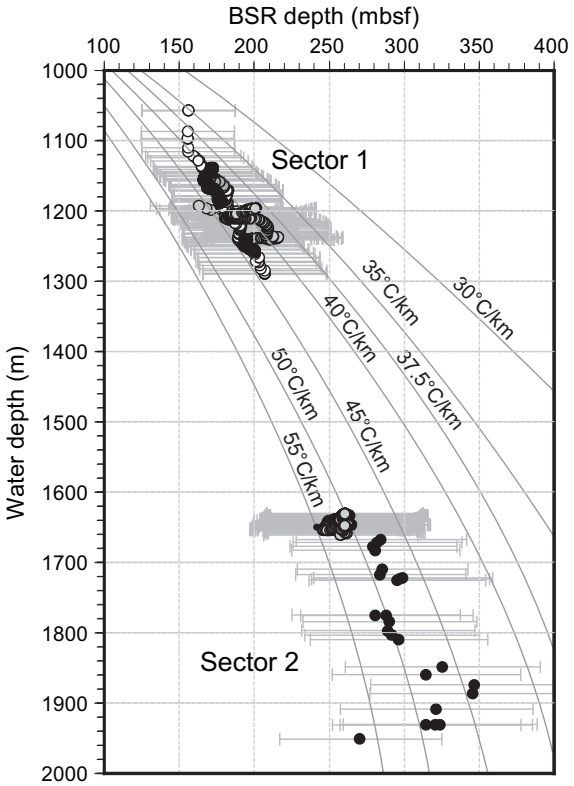

Fig. 9. Cross plots of water depth and BSR depth below the seafloor. Geothermal values computed along seismic lines where BSRs occur in Sectors 1 and 2 are plotted as dots. Horizontal grey bars represent a 20% uncertainty range in the depth conversion of the BSRs. Black curves indicate relationships between theoretical BSR depth and water depth assuming conductive heat flows of 30, 35, 37.5, 40, 45, 50 and 55 °C/km.

4.2. Position of the Indus Fan hydrate system in the global hydrate inventory

The present study shows examples of BSR occurrence on the northern tip of the western Indian rifted margin offshore Pakistan. The BSRs observed adjacent to the present-day Indus Canyon (Sector 2) are comparable setting to the BSR observed by Veerayya et al. (1998) in the Indian deep-water area (Figs. 1 and 2). Sector 1 is the northernmost observed BSR along the margin before the BSRs in the Makran Accretionary Prism observed further west (e.g., White, 1977; Von Rad et al., 2000). Sector 1 shows a very specific tectonic setting, with fluid migration features related to the strike-slip regime along the edge of the plate boundary and gravity collapse/extension driven by the high sedimentation flux from the Indus Delta (Fig. 2).

When these two sectors and other worldwide hydrate province margins are cross plotted together with other margins worldwide with water depth as a function of BSR depth below the seafloor (Fig. 12; Kvenvolden and Claypool, 1988), the observation is that Sectors 1 and 2 are similar to the West African and the Western Indian areas respectively for water depth between 1000 and 2000 m (Cunningham and Lindholm, 2001; Rao et al., 2001) (Fig. 12).

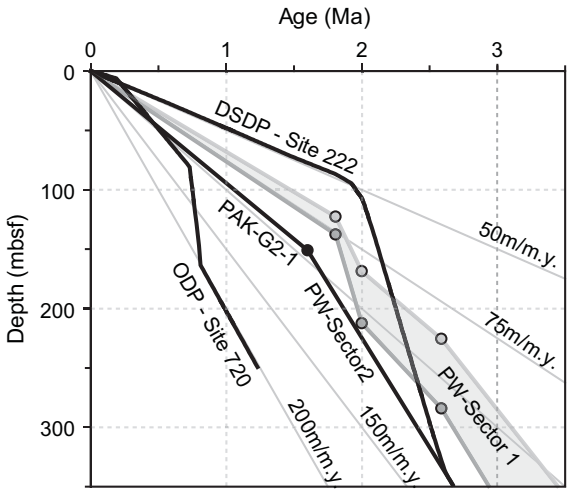

Fig. 10. Sedimentation rates (m/m.y.) at different locations in the study area from boreholes (Black lines: DSDP – Site 222, ODP – Site 720 and PAK-G2-1) and stratigraphic pseudowells (Grey lines: PW-Sectors 1 and 2) from 0 to 3.5 Ma. Well locations can be found in Figs. 1 and 2. Linear sedimentation rates are plotted as thin grey lines ranging from 50 m/m.y. to 200 m/m.y.

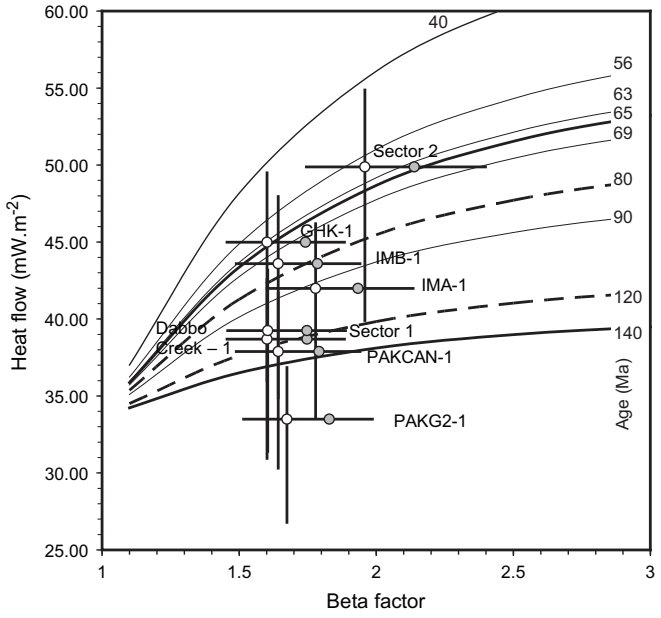

Fig. 11. Heat flow variation with stretching factor (β) of the study area from boreholes (DSDP – Site 222, ODP – Site 720 and PAK-G2-1) and stratigraphic pseudowells (PW-Sectors 1 and 2) from 0 to 3.5 Ma. Location can be found in Figs. 1 and 2. Linear sedimentation rates are plotted as grey lines from 50 m/m.y. to 200 m/m.y. with predicted values for a pure shear model (McKenzie, 1978). Curves are for lithosphere ages and rifting at different major geological events along the Rifted Indian Margin (140 Ma as post break-up of Gondwana, 80–90 Ma as break-up of Madagascar and the Seychelles/India). The last thermal regional event is marked by the curve at 65 Ma corresponding to the Deccan Volcanism with ±2–4 m.y. Error bars represent the beta factors computed with 22, 25 and 27 km crustal thickness, correction of heat flow of 0.8, and 1.1 W m^{-1} K^{-1} thermal conductivity.

It is interesting to compare the tectono-stratigraphic evolution and present-day thermal regime of the Atlantic and Indian Ocean passive margins. Even though the rifting age and tectono-stratigraphy differs, the two margins express common hydrate field stability in the range of 1000–2000 m water depth (Fig. 12). It is unclear which parameters control or influence the hydrate stability field in these different margins, although in these two mature passive margins active tectonism is less important in causing hydrate accumulation, beyond focussing fluid flow in Sector 1. It would be speculative to focus on one process specifically, but we suggest that pressure–temperature conditions and concentration/flux of water-hydrocarbon mixes are the most

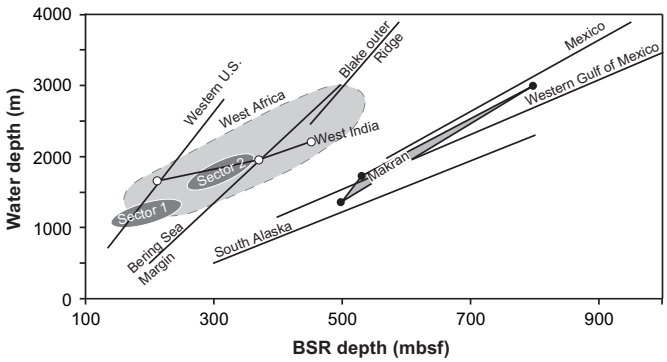

Fig. 12. Location of Sectors 1 and 2 in cross plot of the water-bottom depth and BSR depth below the seafloor for worldwide hydrate provinces (adapted from Kvenvolden and Claypool, 1988; West Africa: Cunningham and Lindholm, 2001; Makran: Von Rad et al., 2000; Grevemeyer et al., 2000; India: Veerayya et al., 1998; Rao et al., 2001).

important controls on the occurrence of hydrates along these margins.

4.3. Thermal regime variation along rifted margins

It is recognized that predicted heat flow spans a range of values, as a result of factors such as the style of rifting, the related heat flow model, as well as the sedimentary and fluid flow history of any given basin (especially sedimentation rate) (Sclater et al., 1981). Heat flow along thermally subsiding passive margins is typically 50 ± 15 mW m^{-2} (e.g. Allen and Allen, 2005). In contrast, oceanic lithosphere of undifferentiated Cenozoic age has variously been estimated to have a mean heat flow of 89.3 mW m^{-2} (Pollack et al., 1993) or 125.2 mW m^{-2} (Stein, 1995). These two model predict values of 44.6 mW m^{-2} and 51.0 mW m^{-2} for Mesozoic oceanic lithosphere. The heat flow compilation of Sclater et al. (1981) for the Indian Ocean indicates the following values for differently aged crust: 65–80 Ma (65 ± 15 mW m^{-2}), 80–95 Ma (52 ± 9 mW m^{-2}), 95–110 Ma (49 ± 8 mW m^{-2}) and 110–125 Ma (50 ± 15 mW m^{-2}). These authors indicate that the low scatter of the data indicated a good fit to the plate model and therefore a decrease in heat flow with increasing oceanic crustal age (i.e. due to plate cooling). The last thermal event at/after rifting (i.e. Deccan volcanism) might be expected to have added heat to the lithosphere, but this also might be obscured is the post-rift structure of the lithosphere equilibrated in less then 100 m.y. (Stein, 1995) or if the thermal blanketing caused by rapid sedimentation was significant (Karner, 1991).

The western Indian rifted margin was affected by the Deccan event dated between 69 and 63 Ma, or over a short period around 65 Ma onshore, with continental flood basalt and a presumed 'offshore' extension being emplaced between 75 and 65 Ma (Courtillot et al., 1999; Malod et al., 1997; Norton and Sclater, 1979). Modern offshore thermal gradients (33–49 °C/km) are indicative of a relatively 'cold', mature regime, according to the heat flow data available (40–70 mW m^{-2}). This situation is consistent with the geodynamic evolution of the area marked by intense volcanic activity at the end of the Cretaceous to Early Tertiary times. In Fig. 11 we show the variation in heat flow versus the degree of continental extension, with much of our Arabian Sea data falling between model rift ages of 120 and 80 Ma (McKenzie, 1978). These older rifting ages correlate with rifting between Madagascar and the Seychelles-India blocks at ~128 Ma and between the Seychelles and India around 85–90 Ma (Norton and Sclater, 1979; Gombos et al., 1995; Collier et al., 2008).

A simple crustal profile derived from the compilation of different data illustrates the potential contribution from crust and mantle radiogenic heating to the thermal regime along a NE–SW transect from the onshore Indus Basin to the deep-sea Indus Fan, assuming that lateral heat conduction is negligible (Fig. 13A and C). This approach has been used on several margins, including the Goban Spur and Galicia Bank (Louden et al., 1991), South Africa (Goutorbe et al., 2008), Congo basin–West Africa (Lucazeau et al., 2004), and the Norwegian margin (Scheck-Wenderoth and Maystrenko, 2008). The crustal thickness is constrained onshore (Kiselev et al., 2007; Kumar et al., 2007), under the continental shelf and slope (MENA 1.1, Walter et al., 2000), and on the oceanic parts of the profile (Gaedicke et al., 2002; Lane, 2006). The transition from radiogenic upper to less thermally productive lower crust between the onshore and the Somnath Ridge is modeled to be 10–15 km deep. Because of the extreme extension, regardless of whether the Somnath Ridge overlies oceanic or continental lithosphere, the choice of exactly where to locate the ocean–continent boundary (OCB) will not drastically affect the predicted crustal heat contribution. Two locations for the OCB are plotted on the crustal regional transect (Fig. 13A). We use known regional crustal heat

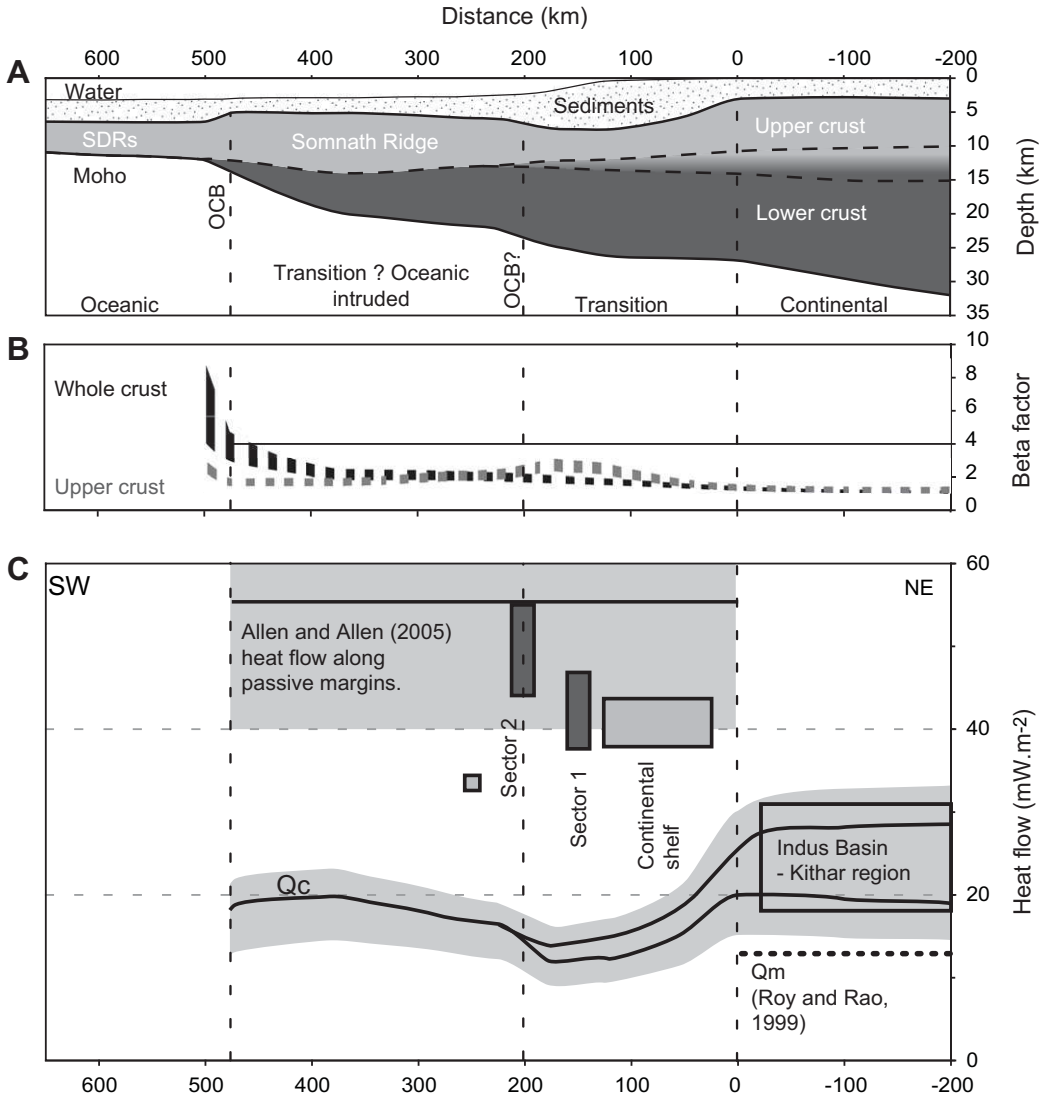

Fig. 13. NE–SW crustal profile from the Indus Basin to the Indus Fan (A) illustrating the variations in the stretching factor (beta) (B), and of the calculated heat flow and estimation of the contribution from crustal radiogenic heating (C) (Qc: crustal, and Qm: mantle radiogenic heat contribution). The coast line is the reference for the distance on- and offshore. Seaward dipping reflections: SDRs.

production (Roy and Rao, 2000), assuming an equivalence between the study area and the Deccan Volcanic Province onshore. The upper crust layer shows values from 1.5 to 2.5 $\mu W\,m^{-3}$ (black curve representing 2.1 $\mu W\,m^{-3}$ in Fig. 13C) and a standard 0.2 $\mu W\,m^{-3}$ is used for the lower crust (Rudnick and Fountain, 1995).

To test the validity of the stretching factor estimated from 1D models (Table 3 and Fig. 11), a 2D estimate is computed along the margin with errors in stretching factor assuming uncertainties of ± 1, ± 2, and ± 2 km for the top basement, Moho and pre-rift crustal thickness respectively. The stretching factors estimated from the 1D thermal models at boreholes or the BSRs geothermal gradient (Fig. 11) are in the range of acceptable uncertainties (± 0.5 beta factor) compared to the crustal 2D model for the margin (Fig. 13B). No major faults are observed on seismic reflection images (cf., large-scale faulting observed at non-volcanic margin, e.g. Galicia Bank, Newfoundland). As a result, the stretching factor cannot be estimated from fault heave and compared to crustal stretching estimates (e.g., Pickup et al., 1996; Reston et al., 1996; Tucholke et al., 2007).

Onshore the predicted crust and mantle radiogenic contribution of 14–17 $mW\,m^{-2}$ in the Indian Shield (Roy and Rao, 2000) is consistent with thermal gradients observed in the Indus Basin (Kithar region) (Fig. 13C). Towards the continental shelf, the observed gradient rises and the crust radiogenic heat contribution falls as the continental crust thins. In order to match the observed values and the radiogenic heat production, at least 10–20 $mW\,m^{-2}$ of heat flux would need to be added from the sediments and/or the mantle. Towards the Somnath Ridge, as the upper crust thins, the crustal heat contribution falls, but although this explains the gradient observed along the margin slope (from BSR estimate) an additional 20–25 $mW\,m^{-2}$ of heat flux would need to be added to the model to match the observations. The Somnath Ridge itself shows a slight increase in upper crust thickness as a result of its magmatic origin. The geothermal gradient observed there is low, possibly because of the occurrence of a carbonate platform overlying the Somnath Ridge basement, acting as an insulator of the crustal radiogenic contribution. Alternatively heat flow may be lower than expected because of the lower radiogenic contribution of extrusive material compared to normal continental crust. More than 15–20 $mW\,m^{-2}$ of additional heat flow is required to reach the observed gradient compared to that predicted from the crustal

model (e.g., potentially from a mantle contribution). Louden et al. (1997) noted that the uniform extension model (McKenzie, 1978) predicts an increase of heat flow with decreasing amount of extension for margins older than 50 Ma. This is in agreement with the observed trend from the Somnath Ridge towards the continental shelf, but is not consistent with the onshore observed heat flow in the Kithar region.

The processes that control variations in thermal gradients along rifted passive margins are still unknown in detail but seem to be mostly related to different crustal domains and age (e.g., crustal composition and rifting age). The continent shows low to medium heat flow values (Precambrian shield). Stretched or transitional crust displays increased heat flow values, with the potential for a higher mantle contribution and a drop of gradient at the transition to oceanic crust (Guillou and Jaupart, 1995; Lucazeau et al., 2004 and reference within). This simple trend seems to be in agreement with the first-order observations of the present study (Fig. 13C), but has yet to be confirmed by denser probe measurements towards the oceanic domain.

5. Conclusion

The regional data synthesis within this paper allows a first-order thermal analysis of the West Indian Rifted Margin. The sparse coverage of probes or deep borehole measurements leads to an initial rough estimate of the thermal regime in the northern portion of the Western Indian Rifted Margin, and raises some questions about the rift initiation considering timing and complexity of the geometry of the margin, as well as the nature of the post break-up sedimentary cover. The thermal event related to emplacement of the Deccan continental flood basalt province at ~65 Ma, and its offshore expression at ~75–65 Ma, does not seem to affect the present-day thermal regime of the margin and surprisingly does not seem to have greatly rejuvenated the rifted lithosphere at the time of emplacement, even though the region was affected by major subsidence anomalies during the Paleogene that are interpreted to be linked to either mantle thermal anomalies, or more likely a thin mantle lithospheric root (Calvès et al., 2008a). This observation suggests that earlier rifting phases pre-dating the break-up of the West Indian Margin from the Seychelles 'micro-continent' are more important in controlling the thermal evolution of the margin. The present-day thermal structure indicates a dominant age of rifting at 120–80 Ma for the rifted continental lithosphere. This study also shows that the lateral discontinuity of BSR occurrence along this margin is possibly related to variations in the host sedimentary systems and/or the occurrence of potential hydrocarbons sources. Further data and measurement from the shallow and deep subsurface should bring more constraints on this simple analysis.

Acknowledgement

The College of Physical Sciences and University of Aberdeen are thanked for the funding, and Shell and the NIO-Pakistan for the data set. Landmark and SMT Kingdom are thanked for their Software University Grants which have allowed this work to take place. This manuscript benefited substantially from reviews by comments from R. Ondrak and F. Lucazeau, and editor H. Verweij.

References

Allen, P.A., Allen, J.R., 2005. Basin Analysis. Principles and Applications, second ed. Blackwell. p. 549.

Bachman, R.T., Hamilton, E.L., 1976. Density, porosity, and grain density of samples from Deep Sea Drilling Project Site 222 (Leg 23) in the Arabian Sea. Journal of Sedimentary Research 46, 654–658.

Bachman, R.T., Hamilton, E.L., 1980. Sediment sound velocities from sonobuoys: Arabian Fan. Journal of Geophysical Research – Solid Earth 85, 849–852.

Bernard, A., Munschy, M., 2000. Le bassin des Mascareignes et le bassin de Laxmi (ocean Indien occidental) se sont-ils formes a l'axe d'un meme centre d'expansion?. (Were the Mascarene and Laxmi Basins (western Indian Ocean) formed at the same spreading centre?) Comptes Rendus De l'Academie Des Sciences – Series IIA/Earth and Planetary Science 330, 777–783.

British Oceanographic Data Centre, 2003. GEBCO Digital Atlas. Centenary Edition [CD-ROM]. Br. Oceanogr. Data Cent., Liverpool, U.K..

Calvès, G., Clift, P.D., Inam, A., 2008a. Anomalous subsidence on the rifted volcanic margin of Pakistan: no influence from Deccan plume. Earth and Planetary Science Letters 272, 231–239.

Calvès, G., Huuse, M., Schwab, A., Clift, P., 2008b. 3D seismic analysis of high-amplitude anomalies in the shallow subsurface of the Northern Indus Fan: sedimentary and/or fluid origin. Journal of Geophysical Research – Solid Earth 113, B11103. doi:10.1029/2008JB005666.

Cande, S.C., Leslie, R.B., Parra, J.C., Hobart, M., 1987. Interaction between the Chile Ridge and Chile Trench: geophysical and geothermal evidence. Journal of Geophysical Research – Solid Earth 92, 495–520.

Christensen, N.I., Mooney, W.D., 1995. Seismic velocity structure and composition of the continental crust: a global view. Journal of Geophysical Research 100, 9761–9788.

Clift, P., Gaedicke, C., 2002. Accelerated mass flux to the Arabian Sea during the middle to late Miocene. Geology 30, 207–210.

Clift, P., Gaedicke, C., Edwards, R., Lee, J.I., Hildebrand, P., Amjad, S., White, R.S., Schlüter, H.-U., 2002. The stratigraphic evolution of the Indus Fan and the history of sedimentation in the Arabian Sea. Marine Geophysical Researches 23 (3), 223–245.

Clift, P.D., 2006. Controls on the erosion of Cenozoic Asia and the flux of clastic sediment to the ocean. Earth and Planetary Science Letters 241 (3–4), 571–580.

Collier, J.S., Sansom, V., Ishizuka, O., Taylor, R.N., Minshull, T.A., Whitmarsh, R.B., 2008. Age of Seychelles–India break-up. Earth and Planetary Science Letters 272, 264–277.

Corfield, R., Carmichael, S., Bennett, J., Akhter, S., Fatimi, M., 2008. Break-up History of a Volcanic Margin: Western India and Pakistan. Rifts Renaissance: Stretching the Crust and Extending Exploration Frontiers. Conference Abstract, Houston, p. 29.

Courtillot, V., Jaupart, C., Manighetti, I., Tapponnier, P., Besse, J., 1999. On causal links between flood basalts and continental breakup. Earth and Planetary Science Letters 166, 177–195.

Courtillot, V., Gallet, Y., Rocchia, R., Féraud, G., Robin, E., Hofmann, C., Bhandari, N., Ghevariya, Z.G., 2000. Cosmic markers, $^{40}Ar/^{39}Ar$ dating and paleomagnetism of the KT sections in the Anjar Area of the Deccan large igneous province. Earth and Planetary Science Letters 182, 137–156.

Cunningham, R., Lindholm, R.M., 2001. Seismic evidence for widespread gas hydrate formation, Offshore West Africa. In: Mello, M.R., Katz, B.J. (Eds.), Petroleum Systems of South Atlantic Margins, first ed. AAPG/Petrobras, pp. 93–105.

Delisle, G., Berner, U., 2002. Gas hydrates acting as cap rock to fluid discharge in the Makran accretionary prism? In: Clift, P.D., Kroon, D., Gaedicke, C., Craig, J. (Eds.), The Tectonic and Climatic Evolution of the Arabian Sea Region Geological Society, London, Special Publications, vol. 195, pp. 137–146.

Deptuck, M.E., Steffens, G.S., Barton, M., Pirmez, C., 2003. Architecture and evolution of upper fan channel-belts on the Niger Delta slope and in the Arabian Sea. Marine and Petroleum Geology 20, 649–676.

Droz, L., Bellaiche, G., 1991. Seismic facies and geologic evolution of the central portion of the Indus Fan. In: Weimer, P., Link, M.H. (Eds.), Seismic Facies and Sedimentary Processes of Submarine Fans and Turbidite Systems. Springer-Verlag, New York, pp. 383–401.

Edwards, R.A., Minshull, T.A., White, R.S., 2000. Extension across the Indian–Arabian plate boundary: the Murray Ridge. Geophysical Journal International 142, 461–477.

Edwards, R.A., Minshull, T.A., Flueh, E.R., Kopp, C., 2008. Dalrymple Trough: an active oblique-slip ocean–continent boundary in the northwest Indian Ocean. Earth and Planetary Science Letters 272, 437–445.

Erickson, S.N., Jarrard, R.D., 1998. Velocity–porosity relationships for water-saturated siliciclastic sediments. Journal of Geophysical Research B: Solid Earth 103, 30385–30406.

Gaedicke, C., Schlüter, H., Roeser, H.A., Prexl, A., Schreckenberger, B., Meyer, H., Reichert, C., Clift, P., Amjad, S., 2002. Origin of the northern Indus Fan and Murray Ridge, Northern Arabian Sea: interpretation from seismic and magnetic imaging. Tectonophysics 355, 127–143.

Gaina, C., Müller, R.D., Brown, B., Ishihara, T., Ivanov, S., 2007. Breakup and early seafloor spreading between India and Antarctica. Geophysical Journal International 170, 151–169.

Gardner, G.H.F., Gardner, L.W., Gregory, A.R., 1974. Formation velocity and density – the diagnostic basics for stratigraphic traps. Geophysics 39, 770–780.

Giles, M.R., Indrelid, S.L., James, D.M.D., 1998. Compaction – the great unknown in basin modeling. In: Geological Society, London, Special Publications, vol. 141 pp. 15–43.

Gombos, A.M., Powell, W.G., Norton, I.O., 1995. The tectonic evolution of western India and its impact on hydrocarbon occurrences: an overview. Sedimentary Geology 96, 119–129.

Goutorbe, B., Lucazeau, F., Bonneville, A., 2008. The thermal regime of South African continental margins. Earth and Planetary Science Letters 267, 256–265.

Grevemeyer, I., Villinger, H., 2001. Gas hydrate stability and the assessment of heat flow through continental margins. Geophysical Journal International 145 (3), 647–660.
Grevemeyer, I., Rosenberger, A., Villinger, H., 2000. Natural gas hydrates on the continental slope off Pakistan: constraints from seismic techniques. Geophysical Journal International 140, 295–310.
Guillou, L., Jaupart, C., 1995. On the effect of continents on mantle convection. Journal of Geophysical Research 100, 217–238.
Henry, S., Danfort, A., Venktraman, S., 2008. Indian Continental Margin: Diachronous Rifting, Ridge Jumps and Continental Fragments. Rifts Renaissance: Stretching the Crust and Extending Exploration Frontiers. Conference Abstract, Houston, p. 102.
Hutchinson, I., 1985. The effects of sedimentation and compaction on oceanic heat flow. Geophysical Journal of the Royal Astronomical Society 82, 439–459.
Hyndman, R.D., Spence, G.D., 1992. A seismic study of methane hydrate marie bottom simulating reflectors. Journal of Geophysical Research 97, 6683–6698.
Japsen, P., Mukerji, T., Mavko, G., 2007. Constraints on velocity–depth trends from rock physics models. Geophysical Prospecting 55, 135–154.
Karner, G.D., 1991. Sediment blanketing and the flexural strength of extended continental lithosphere. Basin Research 3, 177–185.
Kaul, N., Rosenberger, A., Villinger, H., 2000. Comparison of measured and BSR-derived heat flow values, Makran accretionary prism. Pakistan. Marine Geology 164, 37–51.
Khan, M.A., Raza, H.A., 1986. The role of geothermal gradients in hydrocarbon exploration in Pakistan. Journal of Petroleum Geology 9, 245–258.
Kiselev, S., Oreshin, S., Vinnik, L., Gupta, S., Rai, S.S., Singh, A., Kumar, M.R., Mohan, G., 2007. Lithosphere of the Dharwar craton by joint inversion of P and S receiver functions. Geophysical Journal International 173, 1106–1118.
Kolla, V., Coumes, F., 1987. Morphology, internal structure, seismic stratigraphy, and sedimentation of Indus Fan. AAPG Bulletin 71, 650–677.
Kumar, P., Yuan, X., Kumar, M.R., Kind, R., Li, X., Chadha, R.K., 2007. The rapid drift of the Indian tectonic plate. Nature 449, 894–897.
Kvenvolden, K.A., Claypool, G.E., 1988. Gas hydrates in oceanic sediment. U.S. Geological Survey Open-File Report, 88-216, P. 50.
Kvenvolden, K.A., Lorenson, T.D., 2001. The global occurrence of natural gas hydrate. In: Paull, C.K., Dillon, W.P. (Eds.), Natural Gas Hydrates: Occurrence, Distribution, and Detection, first ed. American Geophysical Union, Washington, DC, pp. 3–18.
Lane, C.I., 2006. Rifted margin formation in the northwest Indian ocean: the extensional and magmatic history of the Laxmi Ridge continental margin. Ph.D. thesis, University of Southampton, 182 pp.
Louden, K.E., Sibuet, J.-C., Foucher, J.-P., 1991. Variations in heat flow across the Goban Spur and Galicia Bank continental margins. Journal of Geophysical Research 96, 16131–16150.
Louden, K.E., Sibuet, J., Harmegnies, F., 1997. Variations in heat flow across the ocean–continent transition in the Iberia abyssal plain. Earth and Planetary Science Letters 151, 233–254.
Lucazeau, F., Brigaud, F., Bouroullec, J.L., 2004. High-resolution heat flow density in the lower Congo basin. Geochemistry Geophysics Geosystems 5, Q03001. doi:10.1029/2003GC000644.
Malod, J.A., Droz, L., Kemal, B.M., Patriat, P., 1997. Early spreading and continental to oceanic basement transition beneath the Indus deep-sea fan: northeastern Arabian Sea. Marine Geology 141, 221–235.
Martin, V., Henry, P., Nouzé, H., Noble, M., Ashi, J., Pascal, G., 2004. Erosion and sedimentation as processes controlling the BSR-derived heat flow on the Eastern Nankai margin. Earth and Planetary Science Letters 222, 131–144.
McKenzie, D., 1978. Some remarks on the development of sedimentary basins. Earth and Planetary Science Letters 40, 25–32.
Métivier, F., Gaudemer, Y., Tapponnier, P., Klein, M., 1999. Mass accumulation rates in Asia during the Cenozoic. Geophysical Journal International 137, 280–318.
Minshull, T., White, R., 1989. Sediment compaction and fluid migration in the Makran accretionary prism. Journal of Geophysical Research 94, 7387–7402.
Minshull, T.A., Lane, C.I., Collier, J.S., Whitmarsh, R.B., 2008. The relationship between rifting and magmatism in the northeastern Arabian Sea. Nature Geoscience 1, 463–467.
Miles, P.R., Munschy, M., Segoufin, J., 1998. Structure and early evolution of the Arabian Sea and East Somali Basin. Geophysical Journal International 134, 876–888.
Naini, B.R., Kolla, V., 1982. Acoustic character and thickness of sediments of the Indus Fan and the continental margin of western India. Marine Geology 47, 181–195.
Norton, I.O., Sclater, J.G., 1979. A model for the evolution of the Indian Ocean and the breakup of Gondwanaland. Journal of Geophysical Research 84, 6803–6830.
Pickup, S.L.B., Whitmarsh, R.B., Fowler, C.M.R., Reston, T.J., 1996. Insight into the nature of the ocean–continent transition off West Iberia from a deep multichannel seismic reflection profile. Geology 24, 1079–1082.
Pollack, H.N., Hurter, S.J., Johnson, J.R., 1993. Heat flow from the Earth's interior: analysis of the global data set. Reviews of Geophysics 31, 267–280.
Prell, W.L., Niitsuma, N., et al., 1989. Proc. ODP, Init. Repts., 117. (Ocean Drilling Program), College Station, TX. doi:10.2973/odp.proc.ir.117.1989.
Rao, Y., Subrahmanyam, C., Rastogi, A., Deka, B., 2001. Anomalous seismic reflections related to gas/gas hydrate occurrences along the western continental margin of India. Geo-Marine Letters 21, 1–8.
Rao, H.Y., Subrahmanyam, C., Rastogi, A., Deka, B., 2002. Slope failures along the western continental margin of India: a consequence of gas–hydrate dissociation, rapid sedimentation rate, and seismic activity? Geo-Marine Letters 22, 162–169.
Rastogi, A., Deka, B., Budhiraja, L., Agarwal, G.C., 1999. Possibility of large deposits of gas hydrates in deeper waters of India. Marine Georesources and Geotechnology 17, 49–63.
Reston, T.J., Krawczyk, C.M., Klaeschen, D., 1996. The S reflector west of Galicia (Spain): evidence from prestack depth migration for detachment faulting during continental breakup. Journal of Geophysical Research B: Solid Earth 101, 8075–8091.
Robert, P., 1988. Organic Metamorphism and Geothermal History. Elf-Aquitaine and Reidel Publishing, Dordrecht, 311 p.
Roy, S., Rao, R.U.M., 2000. Heat flow in the Indian shield. Journal of Geophysical Research B: Solid Earth 105, 25587–25604.
Royer, J.-Y., Chaubey, A.K., Dyment, J., Bhattacharya, G.C., Srinivas, K., Yatheesh, V., Ramprasad, T., 2002. Paleogene plate tectonic evolution of the Arabian and Eastern Somali basins. In: Geological Society, London, Special Publication, vol. 195 pp. 7–23.
Rudnick, R.L., Fountain, D.M., 1995. Nature and composition of the continental crust: a lower crustal perspective. Reviews of Geophysics 33, 267–309.
Ruppel, C., 1997. Anomalously cold temperatures observed at the base of the gas hydrate stability zone on the U.S. Atlantic passive margin. Geology 25, 699–702.
Sain, K., Minshull, T.A., Singh, S.C., Hobbs, R.W., 2000. Evidence for a thick free gas layer beneath the bottom simulating reflector in the Makran accretionary prism. Marine Geology 164, 3–12.
Satyavani, N., Thakur, N.K., Aravind Kumar, N., Reddi, S.I., 2005. Migration of methane at the diapiric structure of the western continental margin of India — insights from seismic data. Marine Geology 219, 19–25.
Scheck-Wenderoth, M., Maystrenko, Y., 2008. How warm are passive continental margins? A 3-D lithosphere-scale study from the Norwegian margin. Geology 36, 419–422.
Sclater, J.G., Parsons, B., Jaupart, C., 1981. Oceans and continents: similarities and differences in the mechanisms of heat loss. Journal of Geophysical Research 86, 11535–11552.
Shankar, U., Thakur, N.K., Reddi, S.I., 2004. Estimation of geothermal gradients and heat flow from bottom simulating reflector along the Kerala–Konkan basin of Western Continental Margin of India. Current Science 87, 250–253.
Shankar, U., Thakur, N.K., Ashalatha, B., 2006. Fluid flow related features as an indicator of potential gas hydrate zone: Western continental margin of India. Marine Geophysical Researches 27, 217–224.
Shapiro, N.M., Ritzwoller, M.H., 2004. A global seismic model as proxy for surface heat flux: application to Antarctica. Earth Planetary Science Letter 223, 213–224.
Shipley, T.H., Houston, M.H., Buffler, R.T., Shaub, F.J., McMillen, K.J., Ladd, J.W., Worzel, J.L., 1979. Seismic evidence for widespread possible gas hydrate horizons on continental slopes and rises. AAPG Bulletin 36, 2204–2213.
Shuaib, S.M., Shuaib, S.M.T., 1999. Geology and oil/gas presence in the offshore Indus Basin of Pakistan. In: Meadows, A., Meadows, P.S. (Eds.), The Indus River: Biodiversity, Resources, Humankind, first ed. Oxford University Press, Pakistan, pp. 249–265.
Sloan, E.D., 1998. Clathrate Hydrates of Natural Gases, second ed. Marcel Dekker Inc., New York & Basel, 705 pp.
Stein, C.A., 1995. Heat flow of the earth. In: Ahrens, T.J. (Ed.), A Handbook of Physical Constants: Global Earth Physics. AGU Reference Shelf Series ed., vol. 1. AGU, Washington DC, pp. 144–158.
Stein, C.A., Stein, S., 1992. A model for the global variation in oceanic depth and heat flow with lithospheric age. Nature 359, 123–129.
Storey, M., Mahoney, J.J., Saunders, A.D., Duncan, R.A., Kelley, S.P., Coffin, M.F., 1995. Timing of hot spot-related volcanism and the breakup of Madagascar and India. Science 267, 852–855.
Surya Prakasa Rao, G., Tewari, H.C., 2005. The seismic structure of the Saurashtra crust in northwest India and its relationship with the Rećunion Plume. Geophysical Journal International 160, 318–330.
Todal, A., Eldholm, O., 1998. Continental margin off western India and Deccan Large Igneous Province. Marine Geophysical Researches 20, 273–291.
Tucholke, B.E., Sawyer, D.S., Sibuet, J.-C., 2007. Breakup of the Newfoundland–Iberia rift. In: Geological Society Special Publication, vol. 282 pp. 9–46.
Vanneste, M., De Batist, M., Golmshtok, A., Kremlev, A., Versteeg, W., 2001. Multi-frequency seismic study of gas hydrate-bearing sediments in Lake Baikal, Siberia. Marine Geology 172, 1–21.
Vanneste, M., Poort, J., Batist, M.D., Klerkx, J., 2002. Atypical heat-flow near gas hydrate irregularities and cold seeps in the Baikal Rift Zone. Marine and Petroleum Geology 19, 1257–1274.
Veerayya, M., Karisiddaiah, S.M., Vora, K.H., Wagle, B.G., Almeida, F., 1998. Detection of gas-charged sediments and gas hydrate horizons along the western continental margin of India. In: Geological Society, London, Special Publication, vol. 137 pp. 239–253.
Verzhbitsky, E.V., 2003. Geothermal regime and genesis of the Ninety-East and Chagos-Laccadive ridges. Journal of Geodynamics 35, 289–302.
Von Rad, U., Tahir, M., 1997. Late Quaternary sedimentation on the outer Indus shelf and slope (Pakistan): evidence from high-resolution seismic data and coring. Marine Geology 138, 193–236.
Von Rad, U., Berner, U., Delisle, G., Doose-Rolinski, H., Fechner, N., Linke, P., Lückge, A., Roeser, H.A., Schmaljohann, R., Wiedicke, M., SONNE 122/130 Scientific Parties, Block, M., Damm, V., Erbacher, J., Fritsch, J., Harazim, B.,

Poggenburg, J., Scheeder, G., Schreckenberger, B., von Mirbach, N., Drews, M., Walter, S., Ali Khan, A., Inam, A., Tahir, M., Tabrez, A.R., Cheema, A.H., Pervaz, M., Ashraf, M., 2000. Gas and fluid venting at the Makran accretionary wedge off Pakistan. Geo-Marine Letters 20, 10–19.

Walter, W.R., Pasyanos, M.E., Bhattacharyya, J., O'Boyle, J., 2000. MENA 1.1-An Updated Geophysical Regionalization of the Middle East and North Africa. Lawrence Livermore National Laboratory, 20pp.

White, R.S., 1977. Seismic bright spots in the Gulf of Oman. Earth and Planetary Science Letters 37, 29–37.

White, N., Thompson, M., Barwise, T., 2003. Understanding the thermal evolution of deep-water continental margins. Nature 426, 334–343.

Whitmarsh, R.B., Weser, O.E., Ross, D.A., et al., 1974. Initial Reports of the Deep Sea Drilling Project, vol. 23. U.S. Government Printing Office, Washington. doi:10.2973/dsdp.proc.23.1974, 1180 pp..

Wyllie, M.R.J., Gregory, A.R., Gardner, L.W., 1956. Elastic wave velocities in heterogeneous and porous media. Geophysics 21, 41–70.

Yamano, M., Uyeda, S., Aoki, Y., Shipley, T.H., 1982. Estimates of heat flow derived from gas hydrates. Geology 10, 339–343.